Desalination and Water Treatment
www.deswater.com

doi:10.5004/dwt.2018.21892

103 (2018) 28–39
January

The prediction of cellulose acetate membrane characteristics by recent phenomenological models

Tahereh Jafarpour Check-ab, Zahra Maghsoud*, Seyed Mahmoud Mousavi

Chemical Engineering Department, Faculty of Engineering, Ferdowsi University of Mashhad, Mashhad 9177948974, Iran, Tel. +98 5138805144, Fax +98 5138807186, email: t.jafarpour@mail.um.ac.ir (T. Jafarpour), maghsoud@um.ac.ir (Z. Maghsoud), mmousavi@um.ac.ir (S.M. Movsavi)

Received 19 January 2017; Accepted 5 January 2018

ABSTRACT

Membrane performance in separation processes is strongly dependent on the membrane structure which must be controlled during the formation step. In this study, a mixture of NMP and acetone with different ratios has been utilized as solvent to prepare cellulose acetate membranes with different morphologies. The membranes formed by 0–25% NMP in NMP/acetone mixture had a sponge-like structure with closed pores. By increasing the NMP concentration from 25 to 50%, the morphological structure of membranes changed from sponge-like to finger-like. Results showed that the common thermodynamic and kinetic parameters of membrane formation could not predict the proportion of solvents in which the primary structural change had occurred. Moreover, the analysis of some phenomenological models pertaining to the phase separation process such as Da, η_0/X and $\eta_0/\Delta P$ showed that the recent $\eta_0/\Delta p$ model offered a rather good description of the system morphology with changing mixed solvent composition. A significant finding was that the pure water permeability of membrane was correlated well with the trend predicted by both $\eta_0/\Delta p$ and η_0/X data points.

Keywords: Membrane; Thermodynamic; Kinetic; Morphology

1. Introduction

Membrane technology is increasingly used in a wide range of separation processes. Among different techniques used for fabrication of polymeric membranes, non solvent induced phase separation or immersion precipitation has gained growing acceptance due to its operational simplicity and high flexibility [1]. In this method, the cast polymer solution is introduced into the non solvent bath and due to solvent/non solvent exchange, phase separation occurs leading to the formation of a porous membrane. The membrane performance is mainly determined by the structure obtained during the phase inversion process. Hence, several parameters such as the concentration of polymer in the casting solution [2–4], evaporation time [4], type of non solvent/solvent pairs [5–7] and casting thickness [8,9] affect the final membrane morphology. Among these factors, the selection of non solvent/solvent pair is of great importance. High mutual affinity between solvent and non solvent leads to instantaneous liquid-liquid demixing, which generates porous membrane, whereas in low mutual affinity, a nonporous membrane is obtained due to the delayed onset of demixing [10]. Besides, the membrane morphology could be tuned using a mixture of two solvents with different affinities in the non solvent. Kools [5] studied membrane formation from polysulfone/N-methylpyrrolidone (NMP)-tetrahydrofuran (THF)/water system by changing NMP to THF ratio. The polysulfone/NMP/water systems showed instantaneous demixing, and formed membranes with large macrovoids. On the other hand, polysulfone/THF/water systems revealed delayed demixing and the obtained membranes had a dense close-cell structure. He suggested that an increase in the THF content of the solvent mixture led to a decline in the number of the macrovoids. Shieh and Chung [6] used a mixture of NMP and THF as solvent to prepare cellulose acetate (CA) hollow fiber membranes. In their study, with an increase in THF

*Corresponding author.

content, the size of macrovoids shrank. Li et al. [7] studied CA/NMP-γ-butyrolactone (GBL)/water membrane forming system. Given the poor miscibility of water and GBL, the membranes prepared in this system developed a sponge-like structure. There was also a critical value for the amount of NMP in the solvent mixture (25%), in which the membrane morphology demonstrated a major structural change from finger-like to sponge-like shape. Moreover, Livingston et al. [11] demonstrated that the molecular weight cut-off of polyimide membranes could be controlled by altering solvent mixture composition in polyimide/dimethylformamide (DMF)-dioxane/water dope solution. Maghsoud et al. [12] used THF and DMF solvent mixture for the fabrication of polyvinylchloride (PVC) membranes. In their study, membranes were impermeable to water up to 50 wt.% DMF in the casting solution. Membranes cast at this composition had a typical cellular structure. With an increase in DMF content above 50%, tear-like macrovoids appeared, which shifted into large macrovoids by further rise of DMF amount. Moreover, the cloud points of PVC/DMF-THF/water system moved almost linearly with variation of mixed solvent composition. Therefore, the exact composition of the solvent mixture in which the membrane morphology shifted from sponge-like to finger-like could not be obtained merely by thermodynamics.

Due to the direct impact of membrane structure on its performance, the membrane characteristics can be predicted before preparation with high efficiency in terms of saving time and effort. To predict membrane morphology, it is necessary to study the mechanism of membrane formation by considering thermodynamics and kinetics of the phase inversion process. Thermodynamics involves theoretical construction of the ternary phase diagram or experimental determination of the cloud point data associated with the membrane forming system [12–14]. To study the kinetics of phase separation, composition path on a ternary phase diagram is obtained by solving the mass transfer equations [15]. Some researchers, however, have adopted a simpler approach to the prediction of membrane structure including the employment of phenomenological models. In fact, phenomenological models indicate empirical relationships between thermodynamic or kinetic based parameters, which affect membrane formation. For example, it has been shown that the calculation of apparent diffusion coefficient (D_a) for studying the kinetics of phase separation could be effective in establishing correlations with membrane porosity [16–18].

The X parameter (non solvent affinity with the casting solution) is defined by the following equation:

$$X = \frac{\Delta\delta^2_{p-s}\,\Delta\delta^2_{p-Ns}}{\Delta\delta^2_{s-Ns}} \quad (1)$$

By dividing this parameter to zero shear viscosity of the polymer solution (η_0), Arbab et al. [19] obtained a model to predict porosity. Later, Bazarjani et al. [20] used non solvent osmotic pressure difference between the coagulation bath and polymer solution (ΔP) instead of X parameter, obtaining a more exact model to predict membrane porosity. Recently, Ghasemi and Mohammadi [21] prepared CA membranes from casting solutions which contained different polymer compositions and formamide (cosolvent) to acetone (solvent) ratios (FAR). After a threshold FAR dependent on polymer concentration, the membrane cross-sectional morphology changed from finger-like to sponge-like structure. In their study, the capability of η_0/X and $\eta_0/\Delta p$ models in the prediction of membrane morphology and porosity was investigated. The η_0/X model could predict membrane characteristics, where the marked change in η_0/X Vs FAR curve occurred almost concurrent with the morphology transition from finger-like to sponge-like structure. The overall trend of increased membrane porosity with FAR was also well-predicted by the square root of $\eta_0/\Delta p$. In another study [22], the reliability of the square root of $\eta_0/\Delta p$ in prediction of membrane permeability was also demonstrated.

Some researchers have attempted to predict the membrane performance using morphological characterization [23,24]. Shi et al. [23] created digital membranes by simulation. They studied the effect of membrane morphology on the membrane performance using a 3D model. The information derived from membrane porosity and scanning electron microscopy images were used as model inputs. The simulation results were experimentally verified for both sponge-like and finger-like structures. The water permeation predicted in the simulation revealed good correlation with the experimentally measured results. Nurra et al. [24] proposed a model to predict the flow rate according to the membrane morphological parameters obtained from two-dimensional scanning electron micrographs. In their study, the membrane permeation was calculated in accordance with the numerical membrane morphological parameters in fitting with the Darcy's and Hagen–Poiseuille models. Nevertheless, membrane manufacturers would certainly benefit from using models capable of predicting membrane performance before fabrication.

In this study, we used a mixture of two solvents (NMP and acetone) with different miscibilities with water (non-solvent) to control the CA membrane morphology. We obtained the cloud point curves of the CA/NMP-acetone/water system by changing the mixed solvent composition to investigate the thermodynamics of phase separation. The apparent diffusion coefficient of the non solvent was calculated as a means of studying the kinetics of phase separation. The capability of thermodynamics and kinetics of phase separation, and recent phenomenological models such as η_0/X and $\eta_0/\Delta p$ in prediction of membrane morphology and performance were also evaluated. The main purpose was to analyze the generality of these models; that is, their dependence on the chosen system for membrane formation.

2. Materials and methods

2.1. Materials

CA with acetyl content of 39.8 wt.%, M_n = 30,000 g/mol and density of 1.3 g/cm^3 was purchased from Aldrich Chemical Company. Acetone and 1-methyl-2-pyrrolidone (NMP) with purity of more than 99.5% were supplied by Merck and used as solvents. Tap water was used as coagulant. Sodium chloride (Dr. Mojallali Chemical Complex Co.) was used for preparing salt solution to measure the membrane rejection.

2.2. Preparation of polymer solutions

Homogenous CA/acetone/NMP solutions with various NMP to acetone ratios were prepared in sealed glass bottles at ambient temperature (25 ± 1°C) using a magnetic stirrer for 24 h (see Table 1). After that, they were preserved at room temperature for 4 h to allow the removal of air bubbles.

2.3. Viscosity measurement

Due to high volatility of acetone solvent, conventional rheological instruments such as rotational viscometers could not be used to measure the viscosity of the CA solutions. Therefore, the zero shear viscosity of casting solutions was estimated using a falling ball viscometer. The falling ball experiment is commonly used for determining the viscosity of Newtonian fluids, as it is relatively low-cost and based on a simple theory. Nonetheless, the measurement of non-Newtonian fluids viscosity by the falling-ball viscometer has been reported for low shear rate ranges where the non-Newtonian behaviour could be neglected. In Cho and Hartnett's study [25], the steady shear viscosity of a highly viscoelastic fluid (polyacrylamide solution) at low shear rates was measured using a falling ball viscometer. Results showed a good agreement between viscosity measured by this method and viscosity obtained by the Weissenberg rheogoniometer and capillary viscometer. Later, they studied the feasibility of using falling ball viscometer for non-Newtonian viscosity measurement in the intermediate shear rate range [26]. Their study revealed that viscosity measurement of some non-Newtonian solutions such as Carbopol-960, carboxymethyl cellulose, polyethylene oxide and polyacrylamide with falling ball viscometer was consistent with those obtained from other viscometers.

In this method, the falling velocity of spheres of known size and density is calculated by measuring the time needed for a sphere to fall through a cylindrical tube with fluid. The power-law model [Eq. (2)] is used to obtain the average shear stress (τ):

$$\tau = m\left(\gamma\right)^{n} \tag{2}$$

where m is the fluid consistency coefficient, and γ and n are the shear rate and power law index, respectively.

Table 1
The composition of polymer solutions

CA (wt.%)	Acetone concentration in polymer solution (wt.%)	NMP concentration in polymer solution (wt.%)	NMP concentration in solvent mixture (wt.%)
24	0	76	100
24	19	57	75
24	38	38	50
24	57	19	25
24	76	0	0

With regard to non-Newtonian fluids, the upper and lower bounds of shear stress and shear rate (γ) could be estimated as a function of n using the following polynomial equations [26]:

$$\tau_u = \left(0.2827 + 0.8744n + 0.4562n^2 + 0.7486n^3\right)\frac{2}{9}gR\left(\rho_s - \rho\right) \tag{3}$$

$$\tau_L = \left(0.6388 + 0.6418n - 0.4344n^2 + 0.156n^3\right)\frac{2}{9}gR\left(\rho_s - \rho\right) \tag{4}$$

$$\gamma_u = \left(-1.731 + 41.28n - 116n^2 + 123.9n^3 - 46.72n^4\right)\frac{V_\infty}{R} \tag{5}$$

$$\gamma_L = \left(-2.482 + 54.35n - 160.1n^2 + 178.2n^3 - 69.04n^4\right)\frac{V_\infty}{R} \tag{6}$$

where R is the radius of sphere. ρs, ρ and V_∞ are sphere density, polymer solution density and the terminal velocity in the unbounded case, respectively.

The terminal velocity in the unbounded case (V_∞) is related to the terminal velocity (V) of a sphere falling in a cylinder, which is measured by Faxen equation (Eq. (7)) [27]:

$$V_\infty = \frac{V}{1 - 2.104\frac{R}{R_c} + 2.09\left(\frac{R}{R_c}\right)^3 - 0.95\left(\frac{R}{R_c}\right)^5} \tag{7}$$

where R and Rc are sphere and cylinder radius, respectively.

The power-law index n can be obtained from the following equation [26]:

$$n = \frac{d\left(\mathrm{Ln}R\left(\rho_s - \rho\right)\right)}{d\left(\mathrm{Ln}\left(\frac{V_\infty}{R}\right)\right)} \tag{8}$$

The apparent viscosity η can be calculated as:

$$\eta = \frac{\tau}{\gamma} \tag{9}$$

The viscosity is calculated as the average of upper and lower bounds of viscosity, which could be obtained by averaging the upper and lower bounds of the shear stress and shear rate according to Eqs. (3)–(6). The zero shear viscosity (η_0) is obtainable by extrapolating viscosity-shear rate data to zero shear rate. Here, we used stainless steel spheres of varying diameters in the range of 0.1–0.9 cm. For the purpose of accuracy, all measurements were repeated at least three times and mean values were used. Using a temperature control system (water bath), the temperature during the experiments was maintained at 27 ± 1°C.

2.4. Membrane preparation

CA solutions were cast on a glass plate with a thickness of 150 μm, and then immediately immersed into a water bath at room temperature. The membranes were taken out from the initial water bath and then transferred to a fresh water bath for 24 h to remove the remaining solvents.

2.5. Porosity measurement

For the measurement of porosity, the surface water of wet membranes was removed using a tissue paper and the membranes were weighed (m_w, g). Membranes were then dried in an oven at 80°C and weighed again (m_d). The overall porosity ε (%) was obtained using the following equation [28]:

$$\%\,\varepsilon = \frac{\frac{(m_w - m_d)}{\rho_w}}{\frac{(m_w - m_d)}{\rho_w + m_d}/\rho_p} * 100 \quad (10)$$

where ρ_w and ρ_p are water (1.0 g/cm^3) and polymer density (1.3 g/cm^3), respectively.

2.6. Cloud point curves

Cloud points were determined by visual observation of the turbidity change in the polymer solution. Using a micro pipette, water drops (non solvent) were slowly added to the stirred polymer solution until the solution became turbid. The cloud point was obtained when the turbidity of the solution persisted for at least 5 min. It should be noted that due to high volatility of acetone solvent, for titration of the polymer solution a sealed glass bottle with a small hole on its cap was used. The hole on the bottle cap was opened only for adding non solvent droplets. Polymer solutions were prepared with concentrations of 1, 3, 5 and 7 wt.% and titrated by water as non solvent. To control the temperature of polymer solution, the titration was undertaken in a large water bath container at constant temperature of 25 ± 0.1°C. Cloud points were obtained by calculating the value of different components in the solution [12].

2.7. Apparent diffusion coefficient (D_a)

The apparent diffusion coefficient was calculated based on the wet membrane thickness and the coagulation time. For this purpose, the apparent diffusion coefficient was obtained by dividing the square of wet membrane thickness (d^2) by the coagulation time (t) [18].

$$D_a = \frac{d^2}{t} \quad (11)$$

The coagulation time is defined as the time interval from immersion of the cast solution into the coagulation bath to its detachment from the glass plate. The thicknesses of wet membranes prepared with different solvent ratios were measured using a micrometer. Each measurement was repeated at least three times and the average value was reported.

2.8. Scanning electron microscopy (SEM)

The cross-section images of the membranes were observed using SEM (LEO 1450VP, Germany). Each membrane sample was dried and then fractured in liquid nitrogen. All samples were coated with a thin layer of platinum.

2.9. Evaluation of membrane performance

An ultra filtration setup was used for measuring salt rejection and pure water permeability (PWP) under 6.0 bar of trans-membrane hydraulic pressure. The pure water permeability (PWP) of the membrane was measured using Eq. (12).

$$PWP = \frac{\Delta m / \rho_w}{A\,\Delta t\,\Delta P} \quad (12)$$

where Δm and ρ_w are permeate weight and water density respectively, A is the effective membrane area, Δt is time and ΔP is trans-membrane pressure difference.

NaCl solution (200 ppm) was used as the feed for salt rejection measurements. Salt rejection (R) was calculated by the following equation:

$$R = \left(1 - \frac{C_p}{C_f}\right) * 100 \quad (13)$$

where C_f and C_p are the concentration of NaCl in the feed and permeate, which were determined by conductivity measurements.

2.10. The theoretical binodal curve

The theoretical binodal curve for CA/NMP/water and CA/acetone/water systems were calculated based on the compressible regular solution (CRS) model [29]. This model is only dependent on pure component properties such as mass density, solubility parameter and thermal expansion coefficient without need for estimating or measuring binary or ternary experimental parameters. The CRS model has been proved promising in thermodynamic prediction of membrane morphology [30]. According to this model, the Gibbs free energy of mixing per unit volume (Δg_{mix}) of a ternary polymer mixture is defined as follows [31]:

$$\begin{aligned}\Delta g_{mix} = KT\left(\frac{\varphi_1\tilde{\rho}_1}{N_1\upsilon_1}\ln(\varphi_1) + \frac{\varphi_2\tilde{\rho}_2}{N_2\upsilon_2}\ln(\varphi_2) + \frac{\varphi_3\tilde{\rho}_3}{N_3\upsilon_3}\ln(\varphi_3)\right) + \\ \varphi_1\varphi_2\tilde{\rho}_1\tilde{\rho}_2\left(\delta_{1,0} - \delta_{2,0}\right)^2 + \varphi_1\varphi_2\left(\tilde{\rho}_1 - \tilde{\rho}_2\right)\left(\delta_1^2 - \delta_2^2\right) + \varphi_1\varphi_3\tilde{\rho}_1\tilde{\rho}_3 \\ \left(\delta_{1,0} - \delta_{3,0}\right)^2 + \varphi_1\varphi_3\left(\tilde{\rho}_1 - \tilde{\rho}_3\right)\left(\delta_1^2 - \delta_3^2\right) + \varphi_2\varphi_3\tilde{\rho}_2\tilde{\rho}_3 \\ \left(\delta_{2,0} - \delta_{3,0}\right)^2 + \varphi_2\varphi_3\left(\tilde{\rho}_2 - \tilde{\rho}_3\right)\left(\delta_2^2 - \delta_3^2\right)\end{aligned} \quad (14)$$

where φ_i is the volume fraction of component i with N_i segments of hard core (0 K, zero pressure) volume υ_i. K is the Boltzmann constant and T is the temperature. $\tilde{\rho}_i$ and $\delta_{i,0}$ are the reduced density and hard-core solubility parameter, which are obtained from the hard core density (ρ_i^*) and the component solubility parameter (δ_i) at 298 K, respectively. The details of calculation are given in Ref. [32]. The model input parameters are shown in Table 2.

3. Results and discussion

3.1. Thermodynamics of the phase inversion process

One of the key parameters that affect thermodynamics of the phase inversion process is the non solvent/solvent interaction parameter (g_{12}). The alteration of g_{12} parameter changes the position of the cloud point curve.

3.1.1. The non solvent/solvent interaction parameter (g_{12})

The non solvent/solvent interaction parameter (g_{12}) of water/NMP and water/acetone as a function of solvent volume fraction are depicted in Fig. 1. The data needed to plot g_{12} was taken from references [33,34]. As can be seen, in the entire composition range, the g_{12} values of water/NMP system are lower than those of the water/acetone system, meaning greater miscibility of water and NMP compared to water and acetone. In the literature [7] it has been shown that lower values of g_{12} shift the binodal curve toward the solvent–polymer axis, resulting in lower homogenous regions in the ternary phase diagram. It is confirmed by the theoretical binodal curve plotted for CA/NMP/water and CA/acetone/water (Fig. 2a).

According to Mulder [10], the delayed liquid-liquid demixing and sponge-like structure can be anticipated for the large non solvent/solvent interaction parameter. However, by increasing the miscibility of solvent and non-solvent, i.e. a decrease of g_{12}, membrane porosity rises. Therefore, it is expected that the membranes prepared from water/acetone system develop a sponge-like structure while those prepared from water/NMP contain finger-like macrovoids.

Table 2
Parameters used for calculation of the binodal curve for CA/NMP/water and CA/acetone/water systems[a]

	ρ_i* (g/cm^3)	α (10^{-4} K^{-1})	δ(298K) (Mpa)$^{1/2}$	$N_{Av}\,v$ (cm^3/mol)
CA	1.8	8	25.1	151.2
NMP	1.3	8.4	22.9	75.1
acetone	1.2	13	19.9	50.6
H_2O	1.1	3	47.9	16.7

[a]P-V-T data and solubility parameters from ref [21].

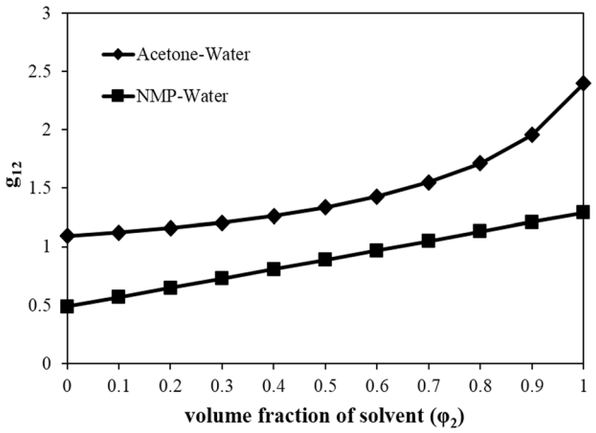

Fig. 1. The nonsolvent/solvent interaction parameter (g12) of water/NMP and water/acetone versus volume fraction of solvent, data taken from ref [27,28].

3.1.2. The cloud point curves

The thermodynamic properties of a membrane forming system could be represented either by experimental cloud points or the theoretical binodal curve. The cloud point data is often restricted to low concentration parts of the phase diagram [32] and the whole phase separation boundary could be depicted by the theoretical binodal curve. As shown in Fig. 2b, the general thermodynamic behavior of both CA/NMP/water and CA/acetone/water systems is relatively well represented, though it does not coincide with the experimental data points. The CRS model used here only takes into account pure component properties [32] and no experimental binary or ternary interaction parameters are utilized as the model input parameters, which might be more fitting with the experimental cloud point data. [35] However, Boom et al. [36] reported that the polydispersity of polymer can undermine the fitness of the cloud point curve with the binodal curve.

Fig. 2a shows the cloud point data of CA/NMP-acetone/water system with different amounts of NMP in the solvent mixture in the range of 0–100 wt.%. As could be

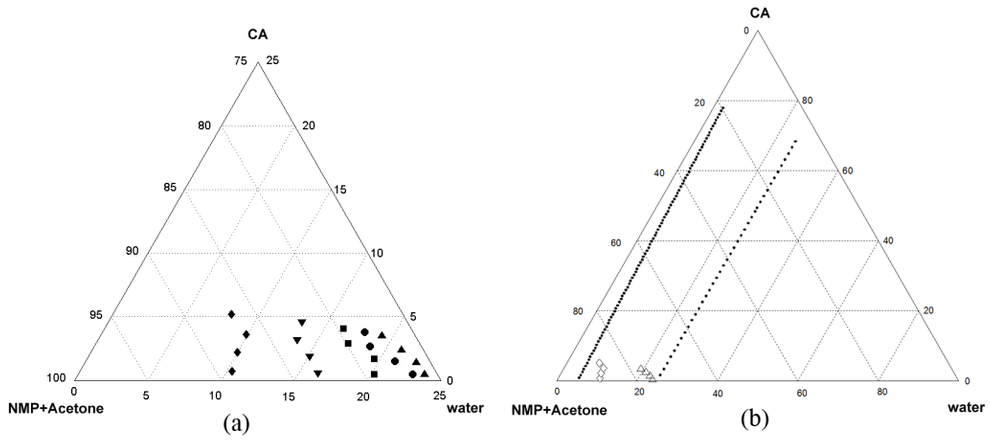

Fig. 2. (a) Cloud point curves as a function of solvent mixture composition (NMP/acetone ratio: ♦ 100/0, ▼ 75/25, ■ 50/50, ● 25/75, ▲ 0/100. (b) Comparison of the cloud point curve and the theoretical binodal curves (dotted lines) for CA/NMP/water (left) and CA/acetone/water (right) systems.

seen, an increase of NMP in the solvent mixture moves the cloud point curve toward the polymer-solvent axis. Therefore, higher amounts of NMP in the solvent mixture obviates the need for large supply of water to initiate phase separation. In the study of Maghsoud et al. [12], the cloud points of PVC/DMF-THF/water system moved linearly with variation of the mixed solvent composition. Therefore, the exact composition of the solvent mixture in which the membrane morphology had changed from sponge-like to finger-like structure could not be estimated. In the present study, however, by increasing the NMP percentage from 50 to 75 wt.%, a greater reduction in the water needed for phase separation was observed. This may be due to major changes in the membrane formation thermodynamics, which could lead to marked morphological changes in the membranes.

3.2. Rheological properties of the casting solutions

Fig. 3 shows the zero shear viscosities of casting solutions containing different compositions of NMP to acetone in the solvent mixture. Solution viscosity plays a major role in membrane formation, as it affects the rate of solvent and nonsolvent exchange. It has been shown that an increase in casting solution viscosity will reduce the tendency for macrovoid formation [2,3,7]. As shown in Fig. 3, by increasing NMP in solvent mixture, the zero shear viscosity rises. Therefore, more NMP content in the solvent mixture slows the exchange rate of solvent and non-solvent and reduces the coagulation rate. On the other hand, given the higher mutual affinity of the NMP/water compared to acetone/water system, a higher coagulation rate is expected by the increased content of NMP in NMP/acetone mixture. Consequently, considering the counter effect of viscosity and solvent/non solvent mutual affinity on the exchange rate of solvent and non-solvent, a conclusive statement about the coagulation rate could not be made without measuring the apparent diffusion coefficient of non-solvent.

3.3. The kinetics of the phase inversion process (the apparent diffusion coefficient)

Fig. 4 shows the apparent diffusion coefficient [D_a, Eq. (11)] calculated for different mixed solvent ratios. By increasing the NMP content in the solvent mixture, the apparent diffusion coefficient (non-solvent diffusion rate) rises. Therefore, it seems that the mutual affinity between solvent and non-solvent dominates the viscosity effect in the exchange rate of solvent and non-solvent. Moreover, there is a steep increase in D_a when NMP content exceeds 50 wt.%. The trend of D_a variation with alteration of NMP percentage is in agreement with system thermodynamics; since the noted change in the position of cloud points was also in the range of 50–75 wt.% NMP.

3.4. Effect of solvent mixture composition on the membrane structure

SEM micrographs of CA membranes are shown in Fig. 5. Different morphologies could be obtained by altering the solvent mixture composition in the cast solution, which runs the gamut from pure acetone to pure NMP. A number of parameters such as the concentration of polymer in the casting solution, the solvent quality and the casting thickness could affect the final membrane morphology [8,9]. There is a critical polymer concentration (C*) in the casting solution above which the finger and void structure disappears. Hung et al. [8] showed that the solvent used to prepare the casting solution had a dramatic effect on the critical concentration. Their results suggested that the casting solutions prepared by the lower quality solvent had a lower critical concentration [8]. In the system of membrane formation in this study, the solubility parameter difference between NMP and CA ($\delta_{CA} - \delta_{NMP} = 2.2$) was lower than acetone and CA ($\delta_{CA} - \delta_{acetone} = 5.2$). Given the lower solvency of acetone for CA, the CA/acetone/water system has a lower critical concentration compared to the CA/NMP/water system.

According to Fig. 5 and as discussed earlier regarding the critical concentration, it could be concluded that the selected polymer concentration (24 wt.%) is between the critical concentrations of the two systems ($C^*_{CA/acetone/water}$ < the selected concentration < $C^*_{CA/NMP/water}$). Moreover, there is a critical casting thickness (L_c) in which the membranes develop a sponge-like structure [9]. In the same vein, according to Fig. 5, a similar conclusion could be made with regard to the selected casting thickness (150 μm), i.e. $L_{c, CA/NMP/water}$ < the selected thickness < $L_{c, CA/acetone/water}$.

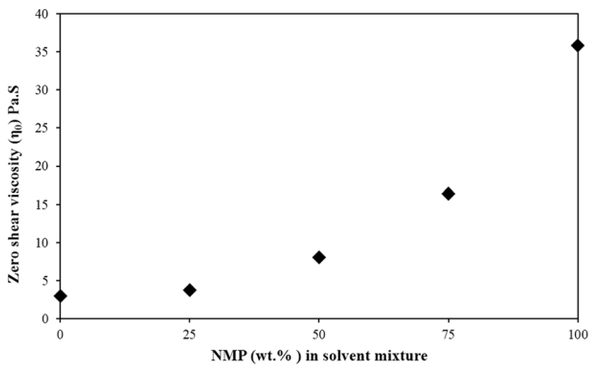

Fig. 3. Zero shear viscosity of CA solutions with different amounts of NMP in the solvent mixture.

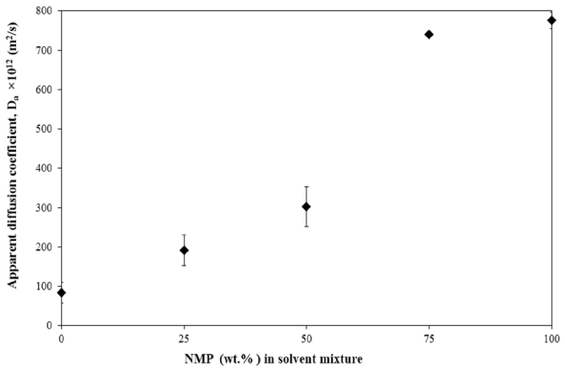

Fig. 4. The apparent diffusion coefficient versus NMP percentage in the solvent mixture.

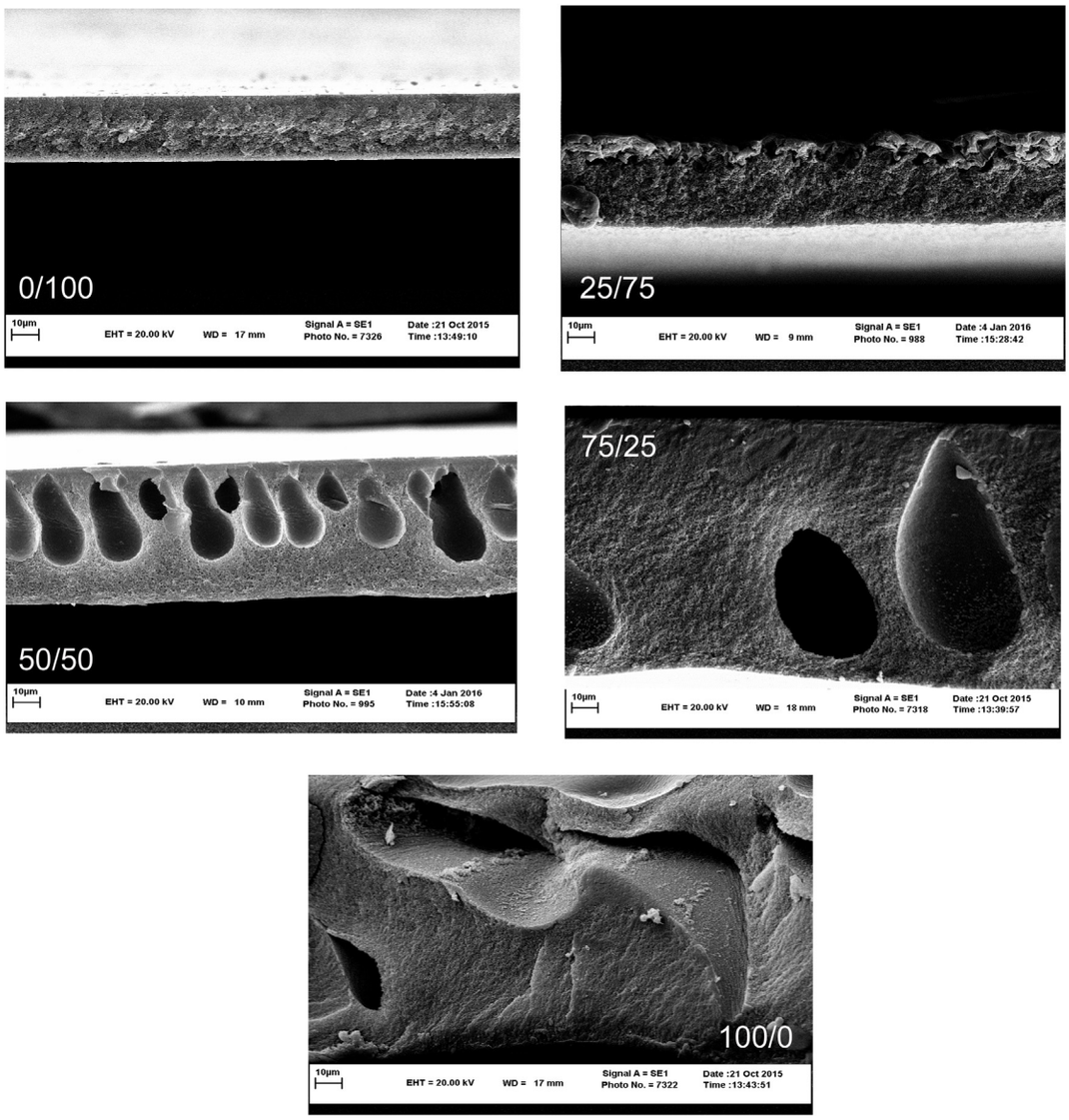

Fig. 5. SEM micrographs of CA membrane cross-sections with different NMP/Acetone ratios (×2000 magnifications).

The membranes prepared from 0 and 25 wt.% NMP typically have a sponge-like structure with closed cell morphology. By further increase in NMP content, finger-like pores appear through the membrane cross-section, with the structure of the spongy part of membranes almost changing from closed-cell pores to open-cell ones (Fig. 6). When the NMP content of the solvent mixture is increased, the nonsolvent affinity toward casting solution is enhanced, so that the phase separation path alters from nucleation and growth of the polymer lean phase to spinodal decomposition and then nucleation and growth of the polymer rich phase. This change in the phase separation mechanism leads to different pore structures [21]. From Table 3, it could be seen that by increasing the NMP concentration in the solvent mixture, the overall porosity and the thickness of membranes rises. The boiling points of acetone and NMP are 56 and 202°C, respectively. Thus, given the greater evaporation in the dope solution with more acetone, a smaller thickness is obtained. In this case, the larger thickness could also be explained in terms of lower membrane shrinkage informed by fast membrane formation, since the outflow of the solvent from the casting solution is lower in this case [37,38].

According to SEM images, there is a marked change in membrane structure from sponge-like to finger-like between 25 and 50 wt.% NMP, whereas the major change in thermodynamics (cloud points) and kinetics (apparent diffusion coefficient) occurs between 50 and 75 wt.% NMP. Therefore, the analysis of thermodynamics and kinetics of the phase inversion process will not be sufficient to predict the exact composition of solvent mixture in which the major structural changes take place. In the next section, the capability of the new phenomenological models such as η_0/X and $\eta_0/\Delta p$ in prediction of membrane structure is investigated.

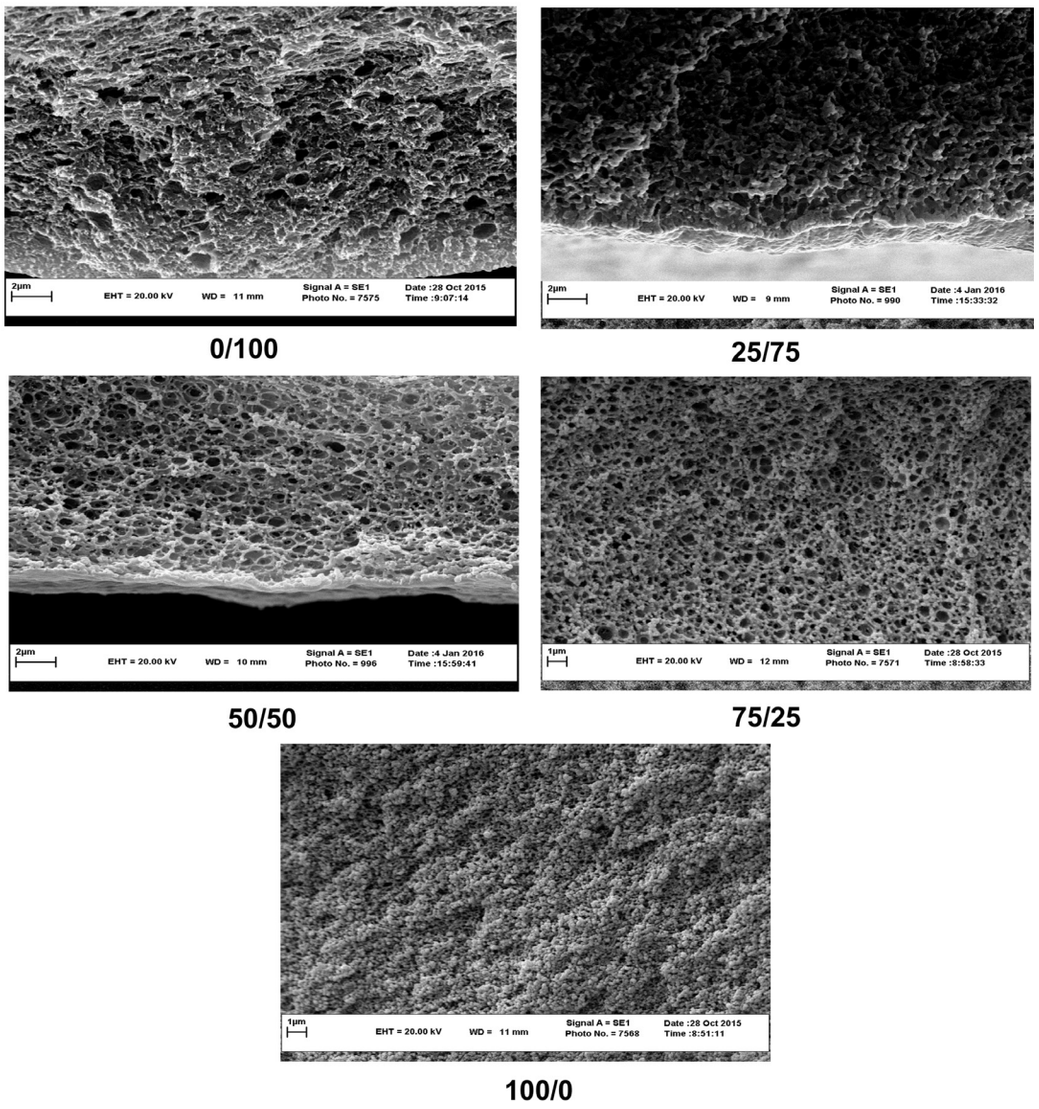

Fig. 6. SEM micrographs of the spongy part of CA membranes with different NMP/Acetone ratios (×15000 magnifications).

Table 3
The overall porosity (ε) and thickness of the membranes prepared from different amounts of NMP in the solvent mixture

NMP in the solvent mixture (wt.%)	0	25	50	75	100
ε (%)	28.0 ± 2.7	66.9 ± 0.4	70.4 ± 0.8	77.0 ± 0.6	78.6 ± 1.3
Membrane thickness (µm)	37.7 ± 6.2	64.3 ± 1.5	81.3 ± 1.5	165.7 ± 3.1	205.0 ± 2.1

3.5. The phenomenological models for the prediction of membrane structure

3.5.1. The η_0/X model

In this model, the zero shear viscosity (η_0) signifies the exchange rate of solvent and non-solvent (kinetics of phase inversion) and the X parameter [according to Eq. (1)] is related to the solubility parameters of the components (phase inversion thermodynamics). Moreover, the η_0/X model has a time dimension, which is a measure of the coagulation time [21]. In Fig. 7, the capability of η_0/X model in prediction of membrane porosity and structure is studied. Although the overall trend predicted by η_0/X is qualitatively consistent with the membrane porosity, it does not display a noticeable

change in the region where the membrane structure changes from sponge-like to finger-like structure, i.e. between 25 and 50 wt.% NMP. However, an obvious increase in the slope of η_0/X data versus NMP content from 50–75 wt.% NMP was observed. In Ghasemi and Mohammadi's study [21], the η_0/X model revealed deviation from initial linearity at the composition of main structural transition. However, the proposed model is not able to give a satisfactory estimation of membrane structural changes informed by alteration of solvent composition in the casting solution.

3.5.2. The $\eta_0/\Delta p$ model

The $\eta_0/\Delta p$ model uses non solvent osmotic pressure difference between the casting solution and coagulation bath (Δp) instead of X parameter adopted in the previous model (η_0/X). The Δp parameter containing binary interaction parameters (χ_{ij}) provides a more comprehensive description of the system thermodynamics. The non solvent osmotic pressure difference (Δp) is calculated by dividing the non solvent chemical potential ($\Delta\mu_1$) by its molar volume (V_1) according to the following equation:

$$\Delta p = -\frac{\Delta\mu_1}{V_1} \tag{15}$$

The non solvent chemical potential ($\Delta\mu_1$) can be obtained from the partial derivative of the Gibbs free energy change of mixing. As proposed by Ghasemi and Mohammadi [21], the CRS model of Mayes was utilized for calculation of $\Delta\mu_1$ [31].

As shown in Fig. 8, the slope change in $\eta_0/\Delta p$ vs. NMP content occurs at the position of membrane structural transition. However, in the case of porosity, only the overall rising trend could be predicted through $\eta_0/\Delta p$ in a qualitative manner. According to the results, it seems that the $\eta_0/\Delta p$ model is superior to other parameters like η_0/X or D_a, as it gives a better picture of the final membrane structure.

3.6. Effect of solvent mixture composition on membrane performance

Table 4 presents the pure water permeability and NaCl rejection of the membranes prepared from different contents of NMP in the solvent mixture. As can be seen, with an increase in NMP percentage in solvent mixture, the pure water permeability is raised due to higher porosity. As for 25 wt.% NMP in the solvent mixture, NaCl rejection could not be measured due to low membrane permeability. By increasing the NMP percentage in the NMP/acetone mixture from 25 to 100 wt.% and changing the sponge-like part of membranes from closed-cell to open-cell, the pure water permeability rises from 0.06 to 1.27 L/(m² h bar). Moreover, informed by greater solvent evaporation, an increase in acetone percentage from 50 to 100 wt.% will make the active layer of membranes denser [38] and raise the salt rejection from 30.7 to 43.7%.

The prediction of membrane structure is beneficial in terms of saving time and energy, but of significant interest is the prediction of membrane performance using simple models. In this section, the trend of changing membrane performance with some phenomenological models such as D_a, η_0/X and $\eta_0/\Delta p$ is evaluated. As shown in Fig. 9, the overall trend of changing the pure water permeability of membranes is predicted by D_a parameter. A similar trend in changing the pure water permeability and D_a parameter has been reported by Yun et al. [16]. Interestingly, by plotting the pure water permeability of membranes and η_0/X or $\eta_0/\Delta p$ versus NMP content in the same figure (Figs. 10 and 11), it was found that the membranes pure water permeability was well-correlated with the trend depicted by both $\eta_0/\Delta p$ and η_0/X data points. In other words, it can be maintained that there is a linear cor-

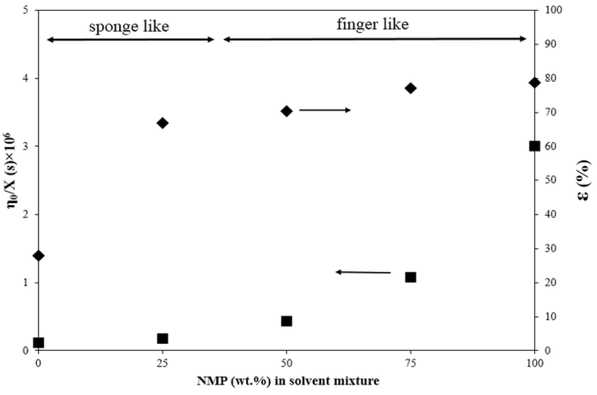

Fig. 7. η0/X and porosity (ε) of the CA membranes as a function of the mixed solvent composition.

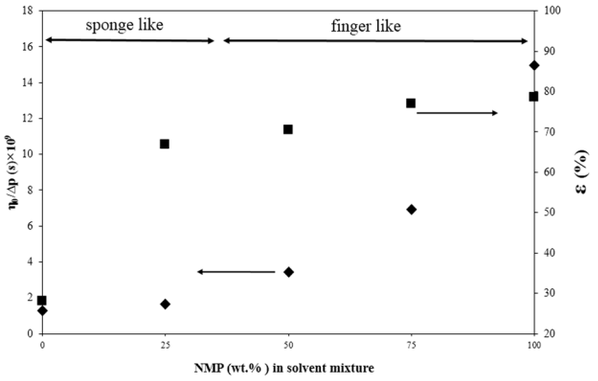

Fig. 8. η0/Δp and porosity (ε) of the CA membranes as a function of the mixed solvent composition

Table 4
The pure water permeability and NaCl rejection of the membranes prepared from different amount of NMP in the solvent mixture

NMP in the solvent mixture (wt.%)	Pure water permeability (L/m² h bar)	NaCl Rejection (%)	Overall porosity (%)
100	1.27 ± 0.14	30.7 ± 2.3	78.6 ± 1.3
75	0.56 ± 0.03	36.1 ± 1.4	77.0 ± 0.6
50	0.26 ± 0.02	43.7 ± 0.9	70.4 ± 0.8
25	0.06 ± 0.01	–	66.9 ± 0.4
0	0	–	28.0 ± 2.7

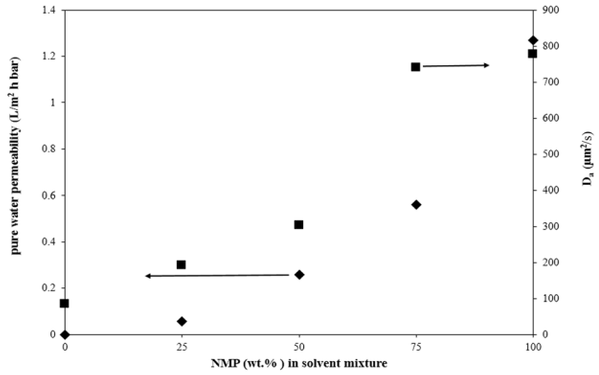

Fig. 9. Membrane pure water permeability and Da versus solvent mixture composition.

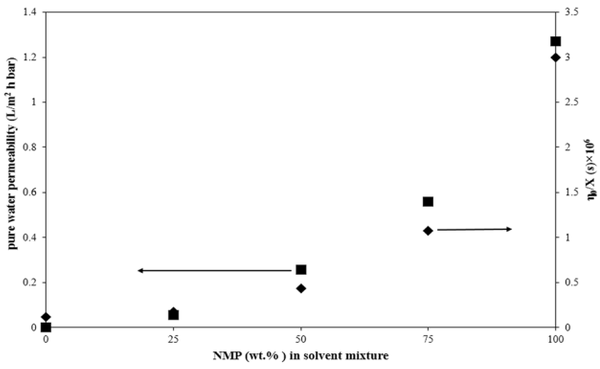

Fig. 10. Membrane pure water permeability and η0/X versus solvent mixture composition.

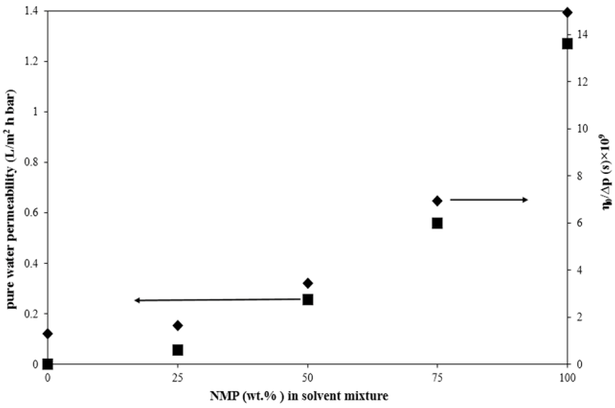

Fig. 11. Membrane pure water permeability and η0/Δp versus solvent mixture composition.

relation between the pure water permeability of membranes and $\eta_0/\Delta p$ or η_0/X data points (Figs. 12 and 13) informed by the variation of NMP in the solvent mixture. The validity of $\eta_0/\Delta p$ and η_0/X models in prediction of pure water permeability was studied with the data provided in the studies of Ghasemi et al. [21], Zhang et al. [39] and Li et al. [7].

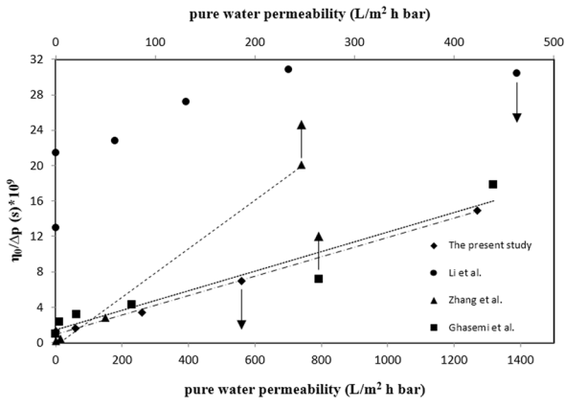

Fig. 12. The η0/Δp versus pure water permeability for four membrane forming systems, polysulfone membranes prepared with different polymer concentrations (Zhang et al. [39]), 20 wt.% CA membranes with different FAR (Ghasemi et al. [21]), CA membranes with different GBL concentrations in solvent mixture (Li et al. [7]) and CA membranes with different mixed solvent compositions prepared in the present study (data multiplied by 103).

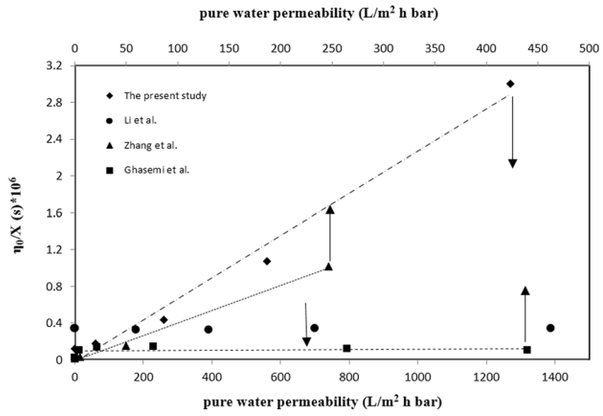

Fig. 13. The η0/X versus pure water permeability for four membrane forming systems, polysulfone membranes prepared with different polymer concentrations (Zhang et al. [39]), 20 wt.% CA membranes with different FAR (Ghasemi et al. [21]), CA membranes with different GBL concentrations in solvent mixture (Li et al. [7]) and CA membranes with different mixed solvent compositions prepared in the present study (data multiplied by 103).

Zhang et al. used different polysulfone concentrations in PSF/N,N-Dimethylacetamide (DMAC)/water system to study the effect of zero shear viscosity on membrane morphology and water flux. As inferred from Figs. 12 and 13, the pure water permeability of membranes measured by Zhang et al. [39] and in the present study changes linearly with both $\eta_0/\Delta p$ and η_0/X data points. However, in the case of 20 wt.% CA membranes with different FAR reported by Ghasemi et al. [21] the $\eta_0/\Delta p$ data points ($R^2 = 0.92$) offer a more suitable measure for predicting membrane performance compared to η_0/X ($R^2 = 0.04$). As discussed in Introduction, Li et al. [7] studied CA/NMP-γ-butyrolactone (GBL)/water membrane forming

system with different GBL concentrations in the solvent mixture. The study of $\eta_0/\Delta p$ and η_0/X models in this membrane forming system showed that neither of these models was able to predict the pure water permeability. In other words, there was no linear correlation between membrane permeability and $\eta_0/\Delta p$ or η_0/X models in this particular membrane forming system.

Moreover, although Gahsemi et al. suggested the use of the square root of $\eta_0/\Delta p$ for the prediction of membrane performance [22], we found that $\eta_0/\Delta p$ provides a proper tool in establishing linear correlations with pure water permeability in some membrane forming systems. This is important as it allows predicting the membrane performance before fabrication in a rather simple way. For this purpose, only the zero shear viscosity (η_0) of the solutions needs to be determined experimentally and Δp or solubility parameter values can be calculated theoretically to give $\eta_0/\Delta p$ or η_0/X as useful guidelines for designing new membranes. However, to select a proper model, it is important to consider the type of membrane forming system to increase the validity of prediction.

4. Conclusions

In the present study, by measuring the thermodynamic and kinetic parameters of the phase inversion process, the mechanism of membrane formation in CA/NMP-acetone/water system was investigated. Moreover, the capability of a number of phenomenological models such as D_a, η_0/X and $\eta_0/\Delta p$ in prediction of membrane structure and performance was evaluated and the following results were obtained:

- An analysis of SEM photographs showed that by increasing the NMP concentration in solvent mixture from 25 to 50 wt.%, a major structural change from sponge-like to finger-like occurred, with the morphology of the spongy part of membranes transforming from closed-cell pores to open-cell ones.
- The membrane prepared from 100% acetone was impermeable in the test pressure range of up to 6 bar. By increasing the NMP percentage in the NMP/acetone mixture from 25 to 100 wt.% and alteration of the spongy part of membranes from closed to open-cell, the pure water permeability was increased from 0.06 to 1.27 $L/(m^2\ h\ bar)$.
- A study of thermodynamics (cloud points) and kinetics (the apparent diffusion coefficient) is not sufficient to predict the structure of membranes as major changes in these parameters were observed by increasing the NMP concentration in solvent mixture from 50 to 75 wt.%.
- The study of some phenomenological models such as D_a, η_0/X and $\eta_0/\Delta P$ in prediction of membrane structure and performance showed that the $\eta_0/\Delta p$ model gave a rather good description of the system morphology with changing mixed solvent composition. In this context, a remarkable finding was that the pure water permeability of membranes was correlated with the trend predicted by both $\eta_0/\Delta p$ and η_0/X data points.
- The validity of $\eta_0/\Delta p$ and η_0/X models was examined for some data obtained from the literature. It was found that the reliability of these models is dependent on the system selected for the membrane formation.

References

[1] G.R. Guillen, Y. Pan, M. Li, E.M.V. Hoek, Preparation and characterization of membranes formed by non solvent induced phase separation: a review, Ind. Eng. Chem. Res., 50 (2011) 3798–3817.
[2] W.Z. Lang, J.P. Shen, Y.T. Wei, Q.Y. Wu, J. Wang, Y.J. Guo, Precipitation kinetics, morphologies, and properties of poly(vinyl butyral) hollow fiber ultrafiltration membranes with respect to polyvinylpyrrolidone molecular weight, Chem. Eng. J., 225 (2013) 25–33.
[3] H. Strathmann, K. Kock, P. Amar, RW. Baker, The formation mechanism of asymmetric membranes, Desalination, 16 (1975) 179–203.
[4] F.J. Paulsen, S.S. Shojaie, W.B. Krantz, Effect of evaporation step on macrovoid defect formation in wet–cast polymeric membranes, J. Membr. Sci., 91 (1994) 265–282.
5] W.F.C. Kools, Membrane Formation by Phase Inversion in Multicomponent Polymer System, Mechanisms and Morphologies, PhD thesis; University of Twente, 1998.
[6] J. Shieh, T.S. Chung, Effect of liquid-liquid demixing on the membrane morphology, gas permeation, thermal and mechanical properties of cellulose acetate hollow fibers, J. Membr. Sci., 140 (1998) 67–79.
[7] Z. Li, J. Ren, A.G. Fane, D.F. Li, F. Wong, Influence of solvent on the structure and performance of cellulose acetate membranes, J. Membr. Sci., 279 (2006) 601–607.[
8] W.L. Hung, D.M. Wang, J.Y. Lai, S.C. Chou, On the initiation of macrovoids in polymeric membranes – effect of polymer chain entanglement, J. Membr. Sci., 505 (2016) 70–81.
[9] D. Li, T.S. Chung, J. Ren, R. Wang, Thickness dependence of macrovoid evolution in wet phase-inversion asymmetric membranes, Ind. Eng. Chem. Res., 43 (2004) 1553–1556.
[10] M. Mulder, Basic Principle of Membrane Technology, Kluwer Academic Publisher, London, 1997.
[11] Y.H. See-Toh, M. Silva, A. Livingston, Controlling molecular weight cut-off curves for highly solvent stable organic solvent nanofiltration (OSN) membranes, J. Membr. Sci., 324 (2008) 220-232.
[12] Z. Maghsoud, M.H. Navid famili, S.S. Madaeni, Preparation of polyvinylcholoride membranes from solvent mixture by immersion precipitation, J. Appl. Polym. Sci., 131 (2014) 40206.
[13] M. Sadrzadeh, S. Bhattacharjee, Rational design of phase inversion membranes by tailoring thermodynamics and kinetics of casting solution using polymer additives, J. Membr. Sci., 441 (2013) 31–44.
[14] J. Han, W. Lee, J.M. Choi, R. Patel, B.R. Min, Characterization of polyethersulfone/polyimide blend membranes prepared by a dry/wet phase inversion: Precipitation kinetics, morphology and gas separation, J. Membr. Sci., 351 (2010) 141–148.
[15] G.R. Fernandes, J.C. Pinto, R. Nobrega, Preparation, modeling and simulation of the phase-inversion process during membrane, J. Appl. Polym. Sci., 82 (2001) 3036–3051.
[16] Y. Yun, P. Le-Clech, G. Dong, D. Sun, Y. Wang, P. Qin, Z. Chen, J. Li, C. Chen, Formation kinetics and characterization of polyphthalazinone ether ketone hollow fiber ultrafiltration membranes, J. Membr. Sci., 389 (2012) 416–423.
[17] X. Li, C. Chen, J. Li, Formation kinetics of polyethersulfone with cardo membrane via phase inversion, J. Membr. Sci., 314 (2008) 206–211.
[18] Q.Z. Zheng, P. Wang, Y.N. Yang, D.J. Cui, The relationship between porosity and kinetics parameter of membrane formation in PSF ultrafiltration membrane, J. Membr. Sci., 286 (2006) 7–11.

[19] S. Arbab, P. Noorpanah, N. Mohammadi, M. Soleimani, Designing index of void structure and tensile properties in wet-spun polyacrylonitrile (PAN) fiber. I. effect of dope polymer or nonsolvent concentration, J. Appl. Polym. Sci., 109 (2008) 3461–3469.
[20] M. Bazarjani, N. Mohammadi, S.M. Ghasemi, Ranking the key parameters of immersion precipitation process and modeling the resultant membrane structural evolution, J. Appl. Polym. Sci., 113 (2009) 1529–1538.
[21] S.M. Ghasemi, N. Mohammadi, The prediction of polymeric membrane characteristics prepared via non solvent induced phase separation by the apparent coagulation time, Polymer, 54 (2013) 4675–4685.
[22] S.M. Ghasemi, N. Mohammadi, The Apparent coagulation time as a tool to predict immersion precipitated polymeric membrane characteristics, The 8th International Chemical Engineering Congress (IChEC), Kish island, Iran, 2014.
[23] M. Shi, G. Printsypar, O. Iliev, V.M. Calo, S.P. Nunes, G.L. Amy, Water flow prediction for membranes using 3D simulations with detailed morphology, J. Membr. Sci., 487 (2015) 19–31.
[24] C. Nurra, L. Pitol-Filho, R. Carraud, S. Pertuz, D. Puig, M.A. Garcia, J. Salvad, C. Torras, Toward the prediction of porous membrane permeability from morphological data, J. Polym. Eng. Sci., (2016) 118–124.
[25] Y.I. Cho, J.P. Hartnett, The falling ball viscometer - a new instrument for viscoelastic fluids, Lett. Heat Mass Transfer, 6 (1979) 335–342.
[26] Y.I. Cho, J.P. Hartnett, W.Y. Lee, Non-new tonian viscosity measurements in the intermediate shear rate range with the falling ball viscometer, J. Non-Newtonian Fluid Mech., 15 (1984) 61–74.
[27] T.A. Butcher, T.F. Irvine, Use of the falling ball viscometer to obtain flow curves for inelastic, non-newtonian fluids, J. Non-Newtonian Fluid Mech., 36 (1990) 51–70.
[28] S. Zhang, K.Y. Wang, T.S. Chung, Y.C. Jean, H. Chen, Molecular design of the cellulose ester-based forward osmosis membranes for desalination, J. Chem. Eng. Sci., 66 (2011) 2008–2018.
[29] A.V.G. Ruzette, A.M. Mayes, A simple free energy model for weakly interacting polymer blends, Macromolecules, 34 (2001) 1894–1907.
[30] S.S. Madaeni, L. Bakhtiari, Thermodynamic-based predictions of membrane morphology in water/dimethylsulfoxide/polyethersulfone systems, Polymer, 53 (2012) 4481–4488.
[31] J.A. Gonzalez-Leon, A.M. Mayes, Phase behavior prediction of ternary polymer mixtures, Macromolecule, 36 (2003) 2508–2515.
[32] Z. Maghsoud, M.H. Navid Famili, S.S. Madaeni, Phase diagram calculations of water/tetrahydrofuran/poly(vinyl chloride)ternary system based on a compressible regular solution model, Iran. Polym. J., 19(8) (2010) 581–588.
[33] L. Zeman, G. Tkacik, Thermodynamic analysis of a membrane forming system water/N-methyl-2-pyrrolidone/polyethersulfone, J. Membr. Sci., 36 (1988) 119–140.
[34] A.J. Reuvers, C.A. Smolders, Formation of membranes by means of immersion precipitation. part II. The mechanism of membranes prepared from the system cellulose acetate- acetone-water, J. Membr. Sci., 34 (1987) 67–86.
[35] Y.M. Wei, Z.L. Xu, X.T. Yang, H.L. Liu, Mathematical calculation of binodal curves of a polymer/solvent/non solvent system in the phase inversion process, Desalination, 192 (2006) 91–104.
[36] R.M. Boom, Th. van den Boomgaard, J.W.A. van den Berg, C.A. Smolders, Linearized cloud point curve correlation for ternary systems consisting of one polymer, one solvent and one non-solvent, Polymer, 34 (1993) 2348–2356.
[37] M.L. Yeow, Y.T. Liu, K. Li, Morphological study of poly (vinylidene fluoride) asymmetric membranes: effects of the solvent, additive, and dope temperature, J. Appl. Polym. Sci., 92 (2004) 1782–1789.
[38] D.Y. Xing, N. Peng, T.S. Chung, Formation of cellulose acetate membranes via phase inversion using ionic liquid, [BMIM] SCN, as the solvent, Ind. Eng. Chem. Res., (2010) 8761–8769.
[39] Z. Zhang, Q. An, Y. Ji, J. Qian, C. Gao, Effect of zero shear viscosity of the casting solution on the morphology and permeability of poly sulfone membrane prepared via the phase-inversion process, Desalination, 260 (2010) 43–50.